MATHEMATICAL BIOSCIENCES
AND ENGINEERING
Volume **1**, Number **1**, June **2004**

http://math.asu.edu/~mbe/

pp. **111–130**

TURING INSTABILITIES AND PATTERN FORMATION IN A BENTHIC NUTRIENT-MICROORGANISM SYSTEM

Martin Baurmann, Wolfgang Ebenhöh and Ulrike Feudel

Institute for Chemistry and Biology of the Marine Environment
Carl von Ossietzky Universität Oldenburg
PF 2503, 26111 Oldenburg, Germany

(Communicated by Yang Kuang)

Abstract. In general, the distributions of nutrients and microorganisms in sediments show complex spatio-temporal patterns, which often cannot be explained as resulting exclusively from the temporal fluctuations of environmental conditions and the inhomogeneity of the studied sediment's material. We studied the dynamics of one population of microorganisms feeding on a nutrient in a simple model, taking into account that the considered bacteria can be in an active or in a dormant state. Using this model, we show that the formation of spatio-temporal patterns can be the consequence of the interaction between predation and transport processes. Employing the model on a two-dimensional vertical domain, we show by simulations which patterns can arise. Depending on the strength of bioirrigation, we observe stripes or "hot spots" (or "cold spots") with high (or low) microbiological activity. A detailed study regarding the effect of non-homogeneous (depth dependent) forcing by bioirrigation shows that different patterns can appear in different depths.

1. **Introduction.** Pattern formation in spatiotemporal systems has been a focus of attention of scientific research since the paper by Turing [32]. He found that the spontaneous emergence of inhomogeneous distributions of chemical substances in reaction-diffusion-systems (RDS) may be of high importance to morphogenetic processes. His seminal paper on diffusion instability was the starting point for a broad theory to establish proof of the significance of pattern formation in a huge class of RDS [21, 20, 19, 24, 28]. The study of chemical RDS showed that pattern formation phenomena will only occur if two nonlinearly reacting chemicals have different diffusion constants (activator and inhibitor). Because this is impossible to achieve in solutions it took three decades to verify Turing's theoretical findings experimentally [7]. Phenomena of pattern formation are not restricted to RDS. Advection also has been identified as a transport process that can induce pattern formation [26, 16, 13, 29, 27]. In particular it has been shown that the instability of a homogeneous distribution of chemical substances can be achieved by the interaction of nonlinear, not necessarily autocatalytic, reactions of three chemical species with advective transport [26]. Furthermore, Henry and Wearne [9] proved

2000 *Mathematics Subject Classification.* 92D25, 92D40.

Key words and phrases. reaction-diffusion models, Turing instability, pattern formation, sediment.

that if anomalous diffusion is taken into account as a transport process, the diffusion coefficients of activator and inhibitor need not to be different to yield Turing instabilities.

Pattern formation was also studied with respect to colonies of microorganisms. Kitsunezaki [12] showed that the surfaces of these colonies can propagate with different velocities, creating a fingering of the moving fronts. He found that this behaviour is a result of the interaction of nonlinear diffusion and an activation mechanism of the bacteria. In a similar way, Tsimring et al. [31] divided bacteria populations into motile and nonmotile parts. In their model, chemotaxis is the process inducing the formation of inhomogeneous distributions. Studying slime mold colonies Camazine et al. [6] showed that chemoattractants (cyclic adenosine monophosphate or cAMP) may play an important role in pattern formation. The same substance was found by Bruns et al. [5, 4] to effect a stimulation of the growth of dormant cells in special planktonic bacteria in fresh and sea water. As the authors state, cAMP or other signal molecules may be relevant to the growth of a broader spectrum of marine bacteria.

The degradation of chemical substances in the sediment is processed by a complex network of different reactions that are mostly controlled by microorganisms [33, 10]. To analyze the essential processes in this network we developed a minimal sediment model (MS-model) that consists of one bacteria population and its (only) nutrient. By studying this model we have shown that pattern formation processes due to diffusion instability can be regarded as one possible mechanism of the formation of inhomogeneous distributions of chemicals found in marine sediments [18, 3, 15]. In [1] we presented a detailed analysis of the dynamical properties of the MS-model in its local form and discussed spatial patterns in 1D (depth in the sediment). Besides that analysis, we used the program CONTENT [14] to compute spatial depth-dependent profiles of chemicals and microorganisms. In particular, we found multistability; that is, the coexistence of different stable spatial patterns.

Based on this previous simplified model we present in this paper a new model, which incorporates on one hand more realistic features motivated by experimental studies, and which is on the other hand considered in a 2D spatial domain. In the model we distinguish between active and dormant bacteria. Degradation is only performed by active bacteria. In our approach, we examine the possibility that the activation of dormant bacteria can be intensified by the active bacteria through the excretion of signal molecules. Another special property of our model is that it is forced by a depth-dependent bioirrigation term. Focusing on the situation in natural systems, we study how the model behaves when we force it by a bioirrigation term that decreases with increasing depth.

The first part of analysis presented in this paper concerns the local model (i.e., only the reaction part of our system). We studied the model behavior for broad ranges of parameters to discover, how environmental influences affect the system. Since we presume that there is a (small) inflow of nutrient and microorganisms, it is guaranteed that none of the species is ever extinct. We found that in almost all cases, the model converges to a steady state, that reacts robustly on changes of the concentrations of the species. The transient behaviour of the model can be characterized by a monotonous convergence toward the equilibrium or an oscillating progression with decreasing amplitude. The steady state is not necessarily unique. It may be accompanied by another equilibrium. In this case the state that is realized over the long term depends on the initial conditions. A special scenario is found

if changes in the environmental conditions (modelled by the parameters) lead to the transition of a stable equilibrium to a repelling focus. In this case, a stable limit-cycle evolves, so that the model's dynamics show stable oscillations.

In section 4 we study the spatial model on a two-dimensional domain. In particular, we analyze the behavior of stationary homogeneous distributions. When studying the stability of the homogeneous solutions, we found that Turing instabilities can occur and spatial patterns evolve over the long term. To study the phenomena of pattern formation we performed several series of computer simulations for certain parameter sets. In a first approach, we study the patterns that evolve when all external forcing is homogeneous. In a second step, we consider parameter sets that are more realistic, taking ito account a depth-dependent forcing. Section 5 is devoted to a discussion of the results.

2. **The setup of the model.** Fig. 1 shows the processes we are taking into account in the model. To implement these processes in a mathematical model, we used the approaches listed in table 1.

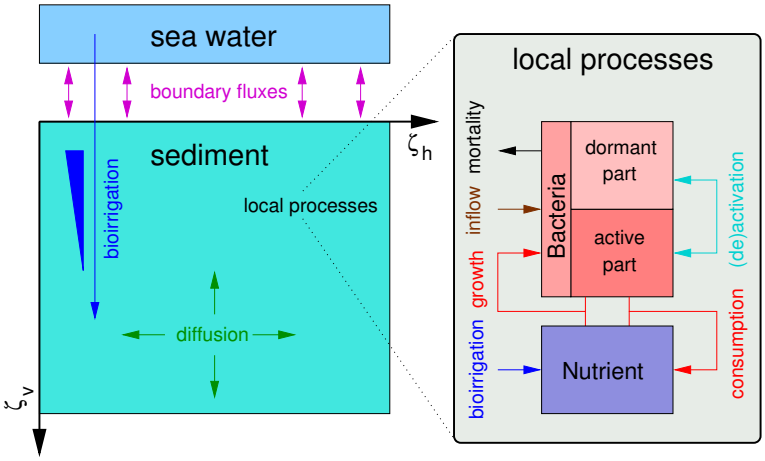

FIGURE 1. The setup of the model.

TABLE 1. Mathematical models for the processes considered.

reaction			non-local transport	local transport
inflow of bacteria (B)	mortality of bacteria (B)	predation (B^{act},N)	bioirrigation (N)	diffusion (B,N)
constant term	linear term	nonlinear term (see text)	depth dep. Fickian flux	Fickian type

The predation term consists of a Holling II function, which is prey-dependent. Since we distinguish between an active and a dormant part of the bacteria population and only the active one contributes to predation, we obtain for the predation term:

$$f_{pred} = X^{act}\frac{Y}{L+Y} = g(X)X\frac{Y}{L+Y}, \tag{1}$$

where X is the population density of the bacteria, X^{act} is the active bacteria, Y the concentration of nutrient, and L the half-saturation constant of the Holling II term. g determines the ratio of active bacteria within the total population. We presume (i) that a certain fraction of bacteria γ is always active and (ii) that an additional activation is induced by the population itself. An appropriate mathematical formulation to implement these features is:

$$g(X) = \gamma + (1-\gamma)\frac{X}{K+X} \tag{2}$$

where K is another half saturation constant and $\gamma \in [0,1]$ is a dimensionless number regulating the strength of active stimulation in comparison to the fixed activity/dormancy ratio.

By these mathematical formulae our PDE-system reads:

$$\begin{aligned}
\frac{\partial X}{\partial \tau} &= \alpha\Big(\gamma + (1-\gamma)\frac{X}{K+X}\Big)\frac{XY}{L+Y} - MX + E + D_X\Big(\frac{\partial^2 X}{\zeta_v^2} + \frac{\partial^2 X}{\zeta_h^2}\Big) \\
\frac{\partial Y}{\partial \tau} &= -\beta\Big(\gamma + (1-\gamma)\frac{X}{K+X}\Big)\frac{XY}{L+Y} + S(\zeta_v)(Y_0 - Y) + D_Y\Big(\frac{\partial^2 Y}{\zeta_v^2} + \frac{\partial^2 Y}{\zeta_h^2}\Big),
\end{aligned} \tag{3}$$

with α and β weighting the influence of predation for bacteria and nutrient. We employ the rate of mortality M, the rate of bacteria inflow E, and the nutrient's concentration in the sea water Y_0. $S(\zeta_v)$ is governing the strength of bioirrigation and D_X, D_Y are the diffusion coefficients for the microorganisms and the chemicals, respectively. We use coordinates $\zeta_{v,h}$ for vertical and horizontal space and τ for time. The bioirrigation corresponds to a nonlocal transport term, which leads to a global coupling of different sites in the system. Any change of the conditions for bioirrigation will affect the nutrient concentrations at any point of the model immediately.

By rescaling, we obtain dimensionless equations with a reduced number of parameters. In particular we apply:

$$\begin{aligned}
t &= \beta\tau & x &= \frac{1}{\beta L}X & y &= \frac{1}{L}Y & z_{v,h} &= \frac{\zeta_{v,h}}{d} & m &= \frac{M}{\beta} \\
\epsilon &= \frac{\alpha}{\beta^2 L}E & k &= \frac{K}{\beta L} & \sigma &= \frac{S}{\beta} & \delta_x &= \frac{1}{\alpha L}D_X & \delta_y &= \frac{1}{\beta L}D_Y,
\end{aligned} \tag{4}$$

where d is the total depth of the model domain.

The substituions yield:

$$\begin{aligned}
\frac{\partial x}{\partial t} &= \Big(\gamma + (1-\gamma)\frac{x}{k+x}\Big)x\frac{y}{1+y} - mx + \epsilon + \delta_x\Big(\frac{\partial^2 x}{z_v^2} + \frac{\partial^2 x}{z_h^2}\Big) \\
\frac{\partial y}{\partial t} &= -\Big(\gamma + (1-\gamma)\frac{x}{k+x}\Big)x\frac{y}{1+y} + \sigma(z_v)(y_0 - y) + \delta_y\Big(\frac{\partial^2 y}{z_v^2} + \frac{\partial^2 y}{z_h^2}\Big).
\end{aligned} \tag{5}$$

3. **Analysis of the local model.** The local model consists of equations (5), not regarding all spatial derivatives and assuming a bioirrigation that is homogeneous in depth. Thus, neglecting the diffusion terms and substituting the function $\sigma(z_v)$ by a fixed parameter σ, we get:

$$\begin{aligned}
\frac{\partial x}{\partial t} &= \Big(\gamma + (1-\gamma)\frac{x}{k+x}\Big)x\frac{y}{1+y} - mx + \epsilon \\
\frac{\partial y}{\partial t} &= -\Big(\gamma + (1-\gamma)\frac{x}{k+x}\Big)x\frac{y}{1+y} + \sigma(y_0 - y)
\end{aligned} \tag{6}$$

To study the equilibria (i.e., the stationary solutions) of the local model, we consider those states in which the time derivatives in equations (6) vanish. In that case we can derive a linear relationship between the coordinates of any equilibrium (x_s, y_s), given by:

$$y = y_0 - \frac{mx - \epsilon}{\sigma} \tag{7}$$

with

$$y \in \Big(0, y_0 + \frac{\epsilon}{\sigma}\Big).$$

Substituting (7) in one of the equations (6) with zero temporal derivatives, we can derive the equilibria. This leads to the problem of finding the roots of the cubic polynomial

$$p(x) := a_3x^3 + a_2x^2 + a_1x + a_0 \tag{8}$$

with the coefficients:

$$\begin{aligned} a_3 &= m(m-1) \\ a_2 &= m^2k - y_0\sigma m + y_0\sigma + \epsilon - 2m\epsilon - m\gamma k - \sigma m \\ a_1 &= \gamma\epsilon - \sigma mk - 2m\epsilon k - y_0\sigma mk + \epsilon^2 + y_0\sigma\gamma k + y_0\sigma\epsilon + \epsilon\gamma k \\ a_0 &= \epsilon k\Big((y_0+1)\sigma + \epsilon\Big). \end{aligned}$$

The roots of the polynomial (8) can be derived analytically but consist of very complex terms. However, we see that—depending on the parameters—there exist one, two, or three positive roots.

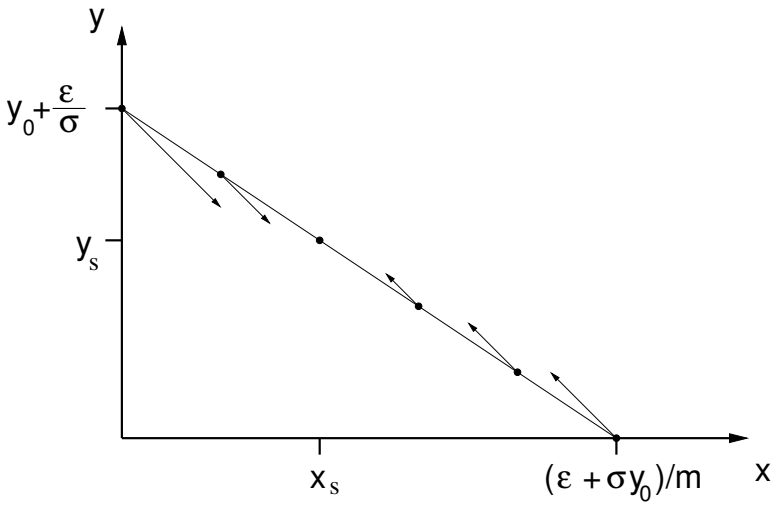

FIGURE 2. The $x+y$-nullcline with velocity vectors. The velocity vectors on the $x+y$-nullcline point in $(1,-1)$ or opposite direction. Straight forward calculus shows us, that at $(0, y_0 + \frac{\epsilon}{\sigma})$ the velocity vector has a southeast direction, wheres at $((\epsilon+\sigma y_0)/m, 0)$ it points to the northwest. Since the change of the velocity vector along the nullcline is continuous, there is in general an odd number of points on the nullcline, in which the velocity vector vanishes.

Referring to (7), we can formulate a more precise statement. For that case, let us consider Fig. 2. The graphics show the $x+y$-nullcline n^* given by (7). Since we

know, that (i) an equilibrium is characterized by a vanishing velocity vector (i.e., $\vec{v} = (\partial x/\partial t, \partial y/\partial t) = 0$), and (ii) that every equilibrium of the system lies on n^*, we find the entire set of equilibria by identifying all points on the nullcline with vanishing velocity-vector. Using this approach, the computation of steady states will be no easier than solving (8). Nevertheless, it allows us to find some basic results. First, we state that any velocity vector on the nullcline obeys:

$$\vec{v} = \frac{\partial y}{\partial t}\begin{pmatrix} -1 \\ 1 \end{pmatrix}. \tag{9}$$

It vanishes, if and only if $\frac{\partial y}{\partial t} = 0$. The nullcline is bounded by the points at which it intersects the axes. At these points, the derivative $\frac{\partial y}{\partial t}$ is easy to compute. We have

$$\left.\frac{\partial y}{\partial t}\right|_{x=0} = -\epsilon \qquad\qquad \left.\frac{\partial y}{\partial t}\right|_{x=\frac{\sigma y_0+\epsilon}{m}} = \sigma y_0. \tag{10}$$

Since $\frac{\partial y}{\partial t}$ is continuous on n^*, the change of signs can only be achieved if there is (i) at least one root of the derivative $\partial y/\partial t$ on the nullcline (ii) in general an odd number of roots on the nullcline (iii) an even number of roots, only in the special case that at least one root of higher order (e.g., a double root) occurs. Keeping in mind, that the roots must also solve (8) we can conclude, that in general we can distinguish between models having one and models having three steady states (see Fig. 3).

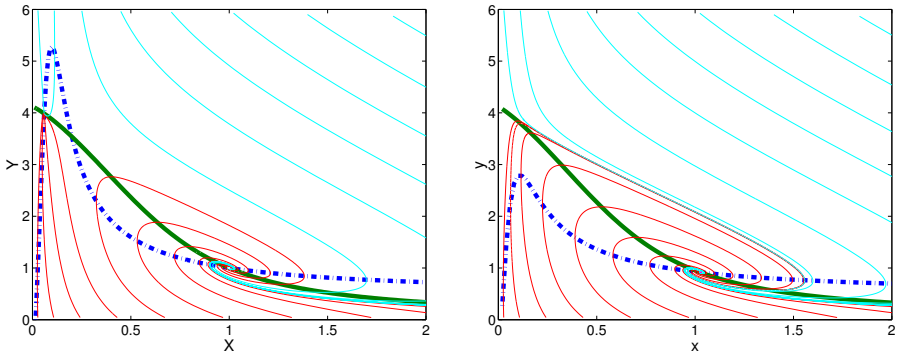

equilibria:
(0.06, 3.99),(0.20, 3.54),(1.0,1.0)

equilibria:
(1.03, 0.91)

FIGURE 3. Nullclines (thick lines; $\frac{\partial x}{\partial t} = 0$ is blue dashed-dotted; $\frac{\partial y}{\partial t} = 0$ is green solid) and trajectories (thin lines) for two systems of different type. We used parameter set 1: $k = 1, \epsilon = 0.005, \sigma = 0.1, m = 0.3175, y_0 = 4.125$. The left plot shows three equilibria; in the right plot, all trajectories converge to a unique steady state. In the left plot, we assumed $\gamma = 0.25$, whereas in the right graph $\gamma = 0.3$. The trajectories start either at $y = 0$ (red) or at $y = 6$ (lightblue).

Fig. (4) illustrates the situation for the continuously changing parameter γ. γ controls the influence of the bacteria's population density on the activation mechanism. If γ is very small, the activation is almost entirely induced by the bacteria.

From a mathematical point of view, the decrease of γ coincides with an increase of the nonlinearity of the system.

It appears, that for a broad range of moderate values γ the system is multistable. This choice of γ corresponds to an existing but weak effect of activation due to signal molecules. As the figure shows, the coexisting stable steady states may be a pair of foci (e.g., at $\gamma = 0.2$), a focus and a node, or (very close to the first saddle-node bifurcation) a pair of nodes.

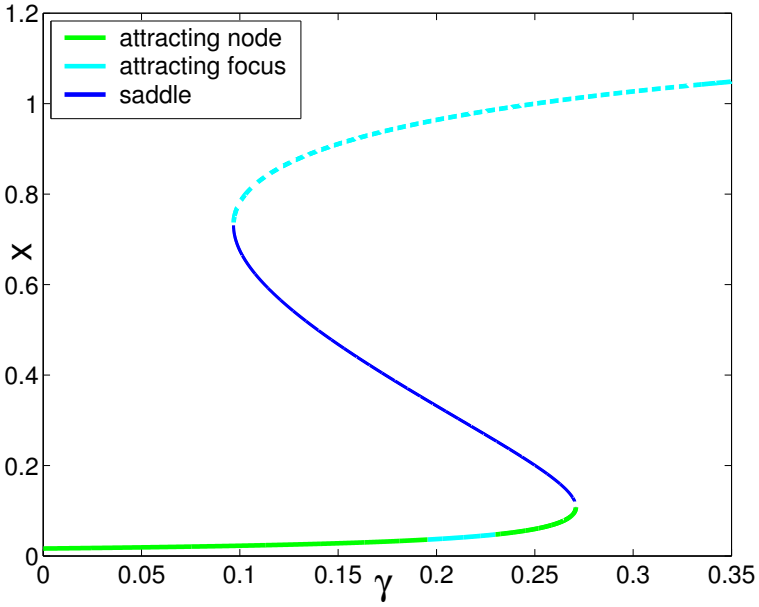

FIGURE 4. Depending on the choice of parameters, the model may have up to three equilibria of different characters. The plot shows all equilibria of a model with the parameters as used for the plots in Fig. 3 and γ being varied. When passing the saddle-node bifurcation at $(\gamma \approx 0.1, x \approx 0.74)$ the saddle turns into an attracting node before changing to an attracting focus. At the chosen resolution the range in which the equilibrium is a node is not visible. (Attracting equilibria characterized by dashed lines are "Turing unstable", we will refer to this in Sect. 4).

We will obtain a different behavior of the system if we consider models with $\sigma = 0.05$. As Fig. 5 shows, at $\gamma \approx 0.29$ the attracting focus loses its stability and becomes a repelling focus. At this point (supercritical Hopf-bifurcation), an attracting limit-cycle evolves (see Fig. 6).

In the phase-plot the trajectories revolve around the focus. In systems having only one equilibrium, they converge to a limit cycle. If the change of γ yields the emergence of another pair of steady states (saddle and attractor), the cycle collides with the saddle and disappears (homoclinic bifurcation). In the corresponding model, the only stable set is then the newly emerged attracting node.

We used analytical methods to determine the stability properties of the steady states based upon the linearization of equations (6). The eigenvalues of these linearized equations derived at the equilibrium points can be used to characterize the

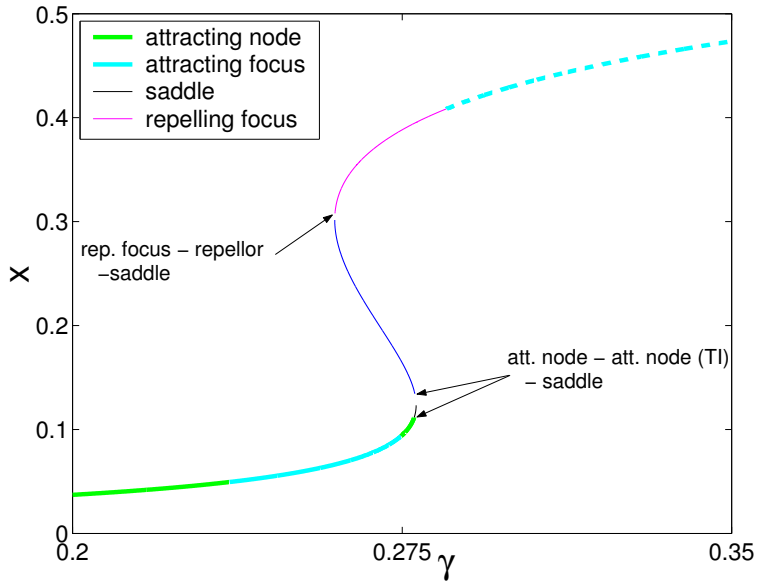

FIGURE 5. Location and characteristics of equilibria existing for models refering to parameter set 2 ($k = 1, \epsilon = 0.005, \sigma = 0.05, m = 0.3175, y_0 = 4.125$). For a broad range of γ there is a repelling focus. Near the saddle node bifurcations the properties of dynamics change very fast so that not all phases can be found at this resolution. For that reason the sequence is given in words.

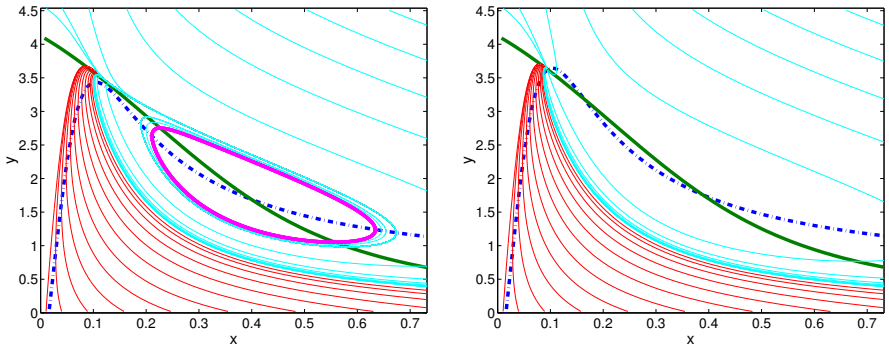

$\gamma = 0.28$ $\gamma = 0.275$

FIGURE 6. In the left plot, all trajectories converge to a limit cycle (pink curve). Decreasing γ, we pass a saddle node bifurcation and we obtain a set of equilibria consisting of a saddle, a repelling focus and an attracting focus. The right plot shows this situation.

dynamics of the system in the neighborhood of the steady state. In particular we

have the following characteristics:

$$\begin{aligned} \Re(\lambda_{loc1}) < 0, \Re(\lambda_{loc2}) < 0 &\qquad \text{attracting equilibrium} \\ \Re(\lambda_{loc1}) < 0, \Re(\lambda_{loc2}) > 0 &\qquad \text{saddle} \\ \Re(\lambda_{loc1}) > 0, \Re(\lambda_{loc2}) < 0 &\qquad \text{saddle} \\ \Re(\lambda_{loc1}) > 0, \Re(\lambda_{loc2}) > 0 &\qquad \text{repelling equilibrium} \end{aligned}$$

We get the eigenvalues $\lambda_{loc1,2}$ by solving

$$\det(\mathbf{J} - \lambda_{loc}\mathbf{I}) = 0, \tag{11}$$

with $\mathbf{J}$ being the Jacobian matrix composed of the derivatives of the right-hand sides of (6) at the steady state (x_s, y_s) under consideration. Equation (11) can be transformed to:

$$\lambda_{loc}^2 - tr(\mathbf{J})\lambda_{loc} + \det(\mathbf{J}) = 0. \tag{12}$$

Hence we obtain:

$$\lambda_{loc}^2 - (A - B - \sigma)\lambda_{loc} + mB - \sigma A = 0 \tag{13}$$

with

$$A = g_x^s \cdot h^s \cdot x_s - \frac{\epsilon}{x_s} \qquad\qquad B = g^s \cdot h_y^s \cdot x_s. \tag{14}$$

and g_x^s and h_y^s given by:

$$g_x^s = \frac{\partial g}{\partial x}\Big|_{x=x_s} = \frac{(1-\gamma)k}{(k+x_s)^2} \qquad\qquad h_y^s = \frac{\partial h}{\partial y}\Big|_{y=y_s} = \frac{1}{(1+y_s)^2} \tag{15}$$

We omit substituting the equilibria's coordinates into (15), because the resulting terms are too complex to tell us very much about the system's behaviour. However, we can compute the eigenvalues $\lambda_{loc1,2}$ analytically and use them to classify the stability of equilibria.

4. **Analysis of the spatial model.** Under certain conditions, reaction-diffusion systems can show the phenomenon of pattern formation. To study whether transport processes can lead to spatially inhomogeneous patterns of chemicals and microorganisms in the sediment, we consider our sediment model on a twodimensional (2D) domain. Besides the reaction part of the model we discussed so far, we will also regard the diffusion terms. The appropriate partial differential equations (PDEs) read:

$$\begin{aligned} \frac{\partial x}{\partial t} &= \Big(\gamma + (1-\gamma)\frac{x}{k+x}\Big)x\frac{y}{1+y} - mx + \epsilon + \delta_x\Big(\frac{\partial^2 x}{z_v^2} + \frac{\partial^2 x}{z_h^2}\Big) \\ \frac{\partial y}{\partial t} &= -\Big(\gamma + (1-\gamma)\frac{x}{k+x}\Big)x\frac{y}{1+y} + \sigma(y_0 - y) + \delta_y\Big(\frac{\partial^2 y}{z_v^2} + \frac{\partial^2 y}{z_h^2}\Big). \end{aligned} \tag{16}$$

First, we identify some properties of the system by a theoretical analysis, considering a model without any nonhomogeneous forcing. We assume, that the biological, chemical, and physical conditions do not depend on space and that there are no non-homogeneous effects induced by boundary conditions (for that purpose let us assume that our domain is infinite).

Of course the homogeneity assumptions do not hold for realistic conditions. To gain insight into realistic cases, we study simulations on a vertical 2D-domain, that is bounded in the second part of this section. Appropriate boundary conditions and the depthdependency of the bioirrigation term will be taken into account explicitly.

4.1. **Stability of homogeneous equilibria in the spatial model.** In contrast to the local model, we employ the spatial model on an (inifinite) 2D domain, so that the steady-state solutions are 2D-functions. First, we want to find the steady-state solutions within a special class of these functions; namely, the homogeneous (i.e. spatially constant) functions (such as $x(z_h, z_v) = c$). Since diffusion flows are driven by spatial gradients, there will be no fluxes in the case of the homogeneous distributions. Thus the homogeneous solutions can be obtained from the solutions of the local model. That means that if $[x_s, y_s]$ is a steady state of (6), the functions $[x_s(z_h, z_v) = x_s, y_s(z_h, z_v) = y_s]$ form an equilibrium with respect to (5). Additionally, we know that no other homogeneous distributions are time-invariant in the spatial model.

Let us now discuss the stability of the homogeneous solutions with respect to perturbations. Turing proved that it is possible for a homogeneous attracting equilibrium to lose stability due to the interaction with diffusion processes. To check under which conditions these Turing instabilities occur in our model, we test how perturbations of a homogeneous steady-state solution behave in the long-term limit. To this end we choose perturbation functions consisting of the following 2D Fourier modes (analogous for $\breve{y}$):

$$\breve{x} = \exp\Big((\kappa_h z_1 + \kappa_v z_2)i + \lambda t\Big). \tag{17}$$

Since we will work with the linearized form of Eq. (5) and the Fourier modes are orthogonal, it is sufficient to analyze the long-term behavior of an arbitrary Fourier mode.

After substituting $x = x_s(z_h, z_v) + \breve{x}$ and $y = y_s(z_h, z_v) + \breve{y}$ in Eq. (5) we linearize the reaction-terms of the equations via a Taylor-expansion about the homogeneous solution. By that transformation we obtain:

$$(\mathbf{J}_{sp} - \lambda\mathbf{I}) \cdot \begin{pmatrix} \breve{x} \\ \breve{y} \end{pmatrix} = 0, \tag{18}$$

with

$$\mathbf{J}_{sp} = \begin{pmatrix} j_{11} - \delta_x(\kappa_h^2 + \kappa_v^2) & j_{12} \\ j_{21} & j_{22} - \delta_y(\kappa_h^2 + \kappa_v^2) \end{pmatrix} \tag{19}$$

and j_{kl} being the entries of the Jacobian matrix J (cf. Eq. 11). Since equation (18) has to be valid for all perturbations we must claim:

$$\begin{aligned} \det(\mathbf{J}_{sp} - \lambda\mathbf{I}) = \lambda^2 + \Big((\delta_x + \delta_y)(\kappa_h^2 + \kappa_v^2) - tr(\mathbf{J})\Big)\lambda + \\ + \det(\mathbf{J}) - (\delta_x j_{22} + \delta_y j_{11})(\kappa_h^2 + \kappa_v^2) + \delta_x\delta_y(\kappa_h^2 + \kappa_v^2)^2 = 0. \end{aligned} \tag{20}$$

As in the local model, the eigenvalues $\lambda_{1,2}$—now dependent on κ_h and κ_v—provide us with the necessary information to determine the stability of the homogeneous equilibrium $[x_s(z_h, z_v), y_s(z_h, z_v)]$. To find Turing instabilities we must focus on the stability properties of the attracting homogeneous solutions $(x_s(z_h, z_v), y_s(z_h, z_v))$. This loss of stability occurs if at least one of the eigenvalues crosses the imaginary axis.

In the spatial model, the value of $\lambda_{1,2}$ depends on the sum of the square of wave numbers $\kappa_h^2 + \kappa_v^2$. Thus both wave numbers affect the eigenvalues. This mathematical property reflects the fact that some Fourier modes will vanish in the long-term limit while others will amplify. To simplify the situation we can make use of $\lambda_{1,2}$ being rotational symmetric functions on the $(\kappa_h, \kappa_v)-$plane. Therefore

we can substitute $\kappa^2 = \kappa_h^2 + \kappa_v^2$ and derive the results for the 2D-case from a 1D-formulation. We have:

$$\lambda^2 - tr(\mathbf{J}_{sp})\lambda + \det(\mathbf{J}_{sp}) = 0 \tag{21}$$

with

$$\begin{aligned} tr(\mathbf{J}_{sp}) &= tr(\mathbf{J}) - (\delta_X + \delta_Y)\kappa^2 \\ \det(\mathbf{J}_{sp}) &= \delta_X\delta_Y\kappa^4 - (\delta_X j_{22} + \delta_Y j_{11})\kappa^2 + \det(\mathbf{J}) \end{aligned} \tag{22}$$

Taking into account that $tr(\mathbf{J}_{sp}) < tr(\mathbf{J})$ we can conclude that for attractors and saddles (both with respect to the local model) a change of stability coincides with a change of the sign of $\det(\mathbf{J}_{sp})$. This change requires that (i) one species x or y is growing autocatalytically and (ii) the autocatalytic species is less mobile than its counterpart (see [19, 24, 1]). Both presumptions are fulfilled in our model: The bacteria grow autocatalytically because of their ability to activate other members of their population by excreting signal molecules. Furthermore, the bacteria are less mobile than the molecules of the nutrient because of their size and because they tend to stick on the sediment matrix. Doing some calculus we find that a change of sign in $\det(\mathbf{J}_{sp})$ occurs when κ takes the critical values

$$\kappa_- = \sqrt{\frac{j_{11}\delta_Y + j_{22}\delta_X - \sqrt{(j_{11}\delta_Y + j_{22}\delta_X)^2 - 4\delta_X^2\delta_Y^2\det(\mathbf{J})}}{2\delta_X\delta_Y}} \tag{23}$$

and

$$\kappa_+ = \sqrt{\frac{j_{11}\delta_Y + j_{22}\delta_X + \sqrt{(j_{11}\delta_Y + j_{22}\delta_X)^2 - 4\delta_X^2\delta_Y^2\det(\mathbf{J})}}{2\delta_X\delta_Y}}. \tag{24}$$

In particular, we have:

$$\det(\mathbf{J}_{sp}) < 0 \qquad \Longleftrightarrow \qquad \kappa_- < \kappa < \kappa_+. \tag{25}$$

If both κ_- and κ_+ exist and have positive values, they limit the range of instability for a locally stable equilibrium. We refer to this range as the *Turing space*. To illustrate these findings, let us consider parameter set 1 (Fig. 3) again and choose $\gamma = 1/4$. Thus the system has three equilibria: $FP_1 = (0.06, 3.99), FP_2 = (0.20, 3.54)$, and $FP_3 = (1.00, 1.00)$. In Fig. 7, the real parts of the eigenvalues of all three equilibria are plotted. Disturbed by a homogeneous perturbation function, the equilibria react like their counterparts in the local model. We can tell by the intersection of the graphs with the $\kappa = 0$ axis what kind of equilibria we find in the local model. Furthermore, Fig. 7(a) shows that FP_1 is unconditionally stable; i.e., perturbations of any wavelength will be damped out. Comparing this plot of eigenvalues with that of FP_2 (Fig. 7(b)), we find that for a saddle there exists a critical bound given by κ_+ below which all perturbations will amplify with time. However, there are—also for a saddle—higher frequences $\kappa > 74.93$ that will be extinguished in the long term. That means that under the influence of diffusion, the attracting character of the saddle is strengthened. Nevertheless, the homogeneous FP_2 equilibrium remains unstable. In Fig. 7(c) we present the typical situation of a Turing instability. With respect to homogeneous perturbations, FP_3 is stable, but increasing κ one eigenvalue changes its sign and we arrive at a range of perturbations inducing the instability of the homogeneous steady state. This Turing space is bounded from above by κ_+.

The change of the bounds κ_- and κ_+ with respect to a variation of γ are illustrated in the left subplot of Fig. 8. Some typical features of Turing spaces in

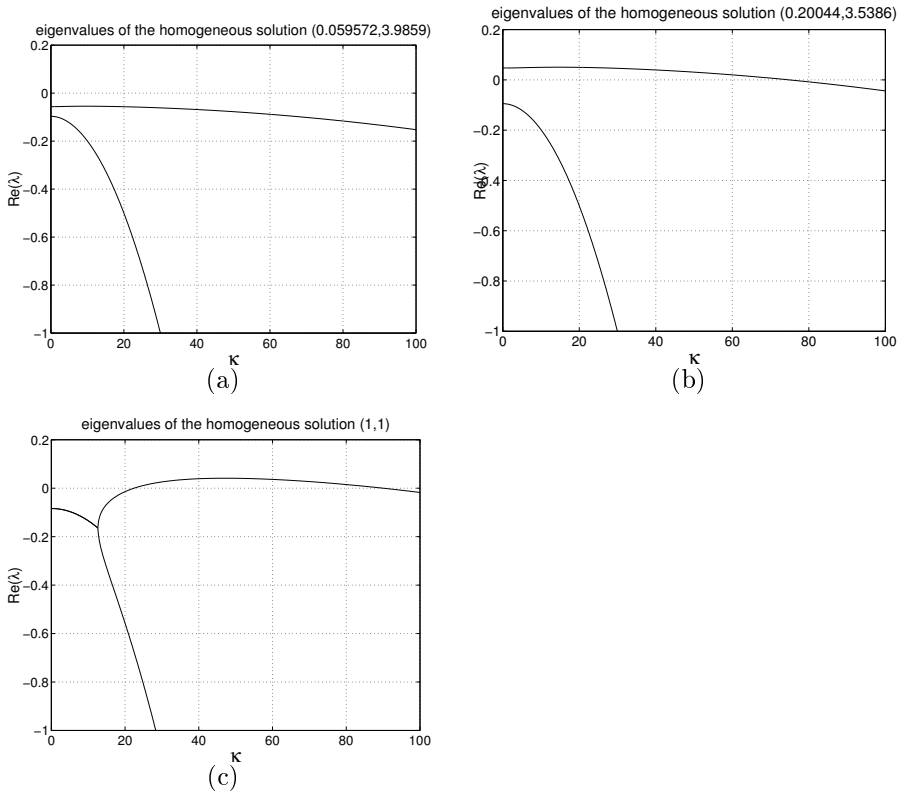

FIGURE 7. Eigenvalues of the equilibria of a model employing parameter set 1 (and $\gamma = 0.25, \delta_X = 10^{-5}, \delta_Y = 10^{-3}$). Disturbed by a homogeneous perturbation function, the equilibria react like their counterparts in the local model. So we can tell by the intersection of the graphs with the $\kappa = 0$ axis what kind of equilibria we find in the local model. As shown above, the character of steady states is given by the sequence: (a) attracting node (real eigenvalues with negative realparts); (b) saddle (real eigenvalues with different signs); (c) attracting focus (complex eigenvalues with negative realparts).

our model can be observed in that plot: The Turing space is limited by two different bounds. On the right side the curves indicating κ_+ and κ_- converge in one point. Beyond that bound, FP_3 exists further but is unconditionally stable. The left bound of the Turing-space shows an "open end". The κ_- curve hits the γ-axis, whereas—at the same γ—the graph of κ_+ returns and continues as the κ_+ curve of FP_2. This bound corresponds to the saddle-node at $(\gamma = 0.097, x = 0.74)$ in the bifurcation plot, and the equilibrium FP_3 does not exist beyond this bound.

When we increase δ_X, the Turing-spaces of the attractors are getting smaller. For the right plot in Fig. 7, we chose $\delta_Y = \delta_X = 10^{-3}$, and the isolines $\det(\mathbf{J}_{sp}) = 0$ consist only of the κ_+ graph belonging to FP_2. Thus no Turing-instabilities can occur if the diffusion coefficients are equal.

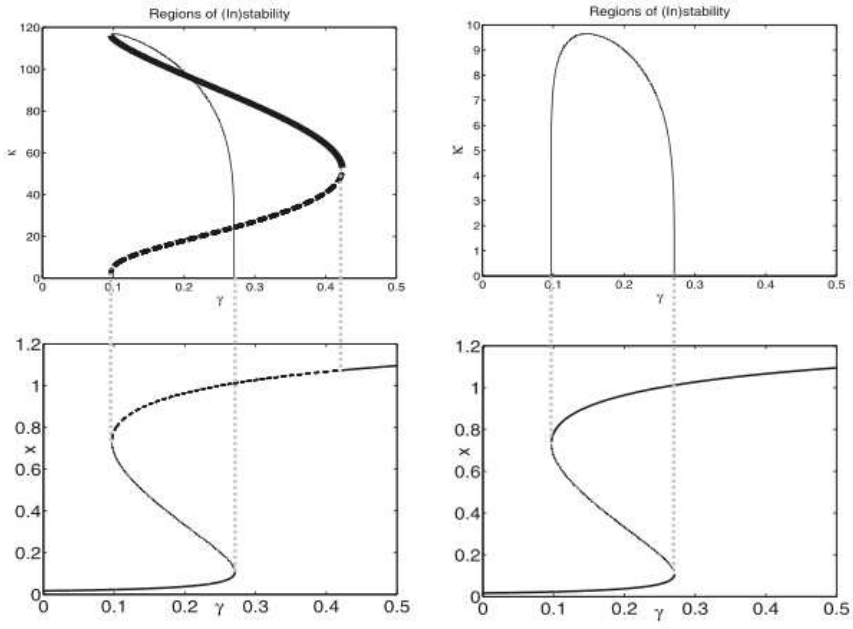

FIGURE 8. Plots of Turing-spaces (above) and bifurcation diagrams (below) for $\delta_X = 10^{-5}, \delta_Y = 10^{-3}$ (right) and $\delta_X = \delta_Y = 10^{-3}$ (left). In the Turing-space plots the κ_+ (solid lines) and κ_- (dotted lines) curves of FP_2 (thin lines) and FP_3 (thick lines) are shown. There is also a range of instability for FP_1, but it is too small to be seen at this resolution. If $\delta_X = \delta_Y$ (right) no ranges of instability corresponding to FP_1 or FP_3 exist.

4.2. **Pattern formation in sediments attributable to Turing instabilities.** To study how structures in the sediment model evolve and to what patterns they converge, we performed several series of computer simulations. We simulate the dynamics of nutrient and bacteria on a two-dimensional horizontal-vertical model domain that has the length 1.3 and the depth 1.0 (both dimensionless lengths).

4.2.1. *Models forced by uniform bioirrigation.* Performing the first series of simulations we assume that the homogeneous $[x_s, y_s]$-distributions (with $[x_s, y_s]$ being an attracting state in the local model) are stationary. Thus we neglect nonuniform bioirrigation by setting $\sigma(z_v) = \sigma = const$ and formulate appropriate boundary conditions: We presume to have periodic boundary conditions at the boundaries $z_h = 0$ and $z_h = 1.3$. At the bottom of the domain ($z_v = 1.0$), there shall be no fluxes; at the top ($z_v = 0$) we assume that the values of $x = x_s$ and $y = y_s$ do not change with time. We start each simulation assuming that it is in the homogeneous $[x_s, y_s]$-equilibrium. To induce a dynamics that may lead to pattern formation, we perturb the x-distribution by small random values.

Fig. 9 shows a stationary pattern that emerges in the distribution of the bacteria's population density. The y-profile corrsponding to the nutrient distribution

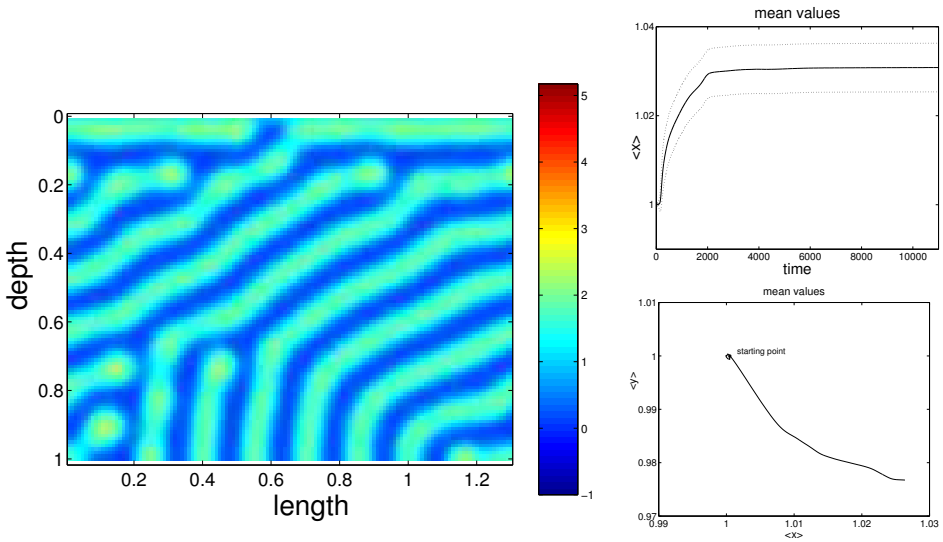

(a) (b)

FIGURE 9. (a) Stationary state of the 2D-simulation basing on parameter set 1, $k = 1, \delta_X = 2 \cdot 10^{-5}$ and $\delta_Y = 10^{-3}$. The simulation exhibits structures that could be regarded as wormholes. (b) The temporal development of the spatial average and variance of x plotted against time (top) the temporal development of the mean in the pseudo state-space (below).

appears qualitatively as the inverse of the bacteria-distribution. Both are characterized by strip-formed structures, which are horizontally oriented at the top and vertically orientated at the bottom. This different orientation is due to the different boundary conditions at the top and the bottom of the domain. Between the depth of 0.2 and 0.8, we have a region with inclined stripes; below that, the structures are almost vertical. The transitions from one zone to the other are rather abrupt. Some stripes have dead ends in which the concentration of nutrient is increased.

The temporal development of the spatially averaged values of the bacteria's population density (Fig. 9 (b)) shows that in the first intervalls of simulation these values change fast and the variance increases. At $t \approx 2000$, the variance reaches a constant value and the mean increases slower. At this time the pattern has almost completely evolved. At $t > 8000$ the system has reached its steady state.

The pattern illustrated in Fig. 9 is not the only inhomogeneous structure that can evolve in the sediment model. Varying the strength of bioirrigation (parameter σ) we obtain three different types of patterns. Similar patterns have also been found in other two-dimensional activator-inhibitor systems, such as the Brusselator (see [22, 11]). Fig. 10 illustrates the dependency of structures with respect to changes in σ. For small values of σ (e.g., $\sigma = 0.05$), i.e. low inflow of nutrient, the homogeneous steady state is characterized by a low density of bacteria. It cannot be destabilized by perturbations. Increasing σ, the local model becomes bistable and a homogeneous equilibrium with higher population densities occurs. This homogeneous profile is unstable, and in the long run a pattern with isolated

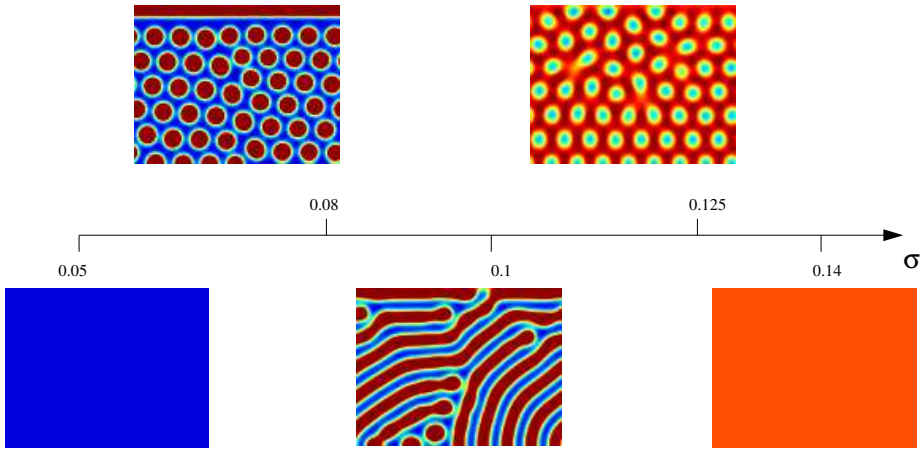

FIGURE 10. Inhomogeneous patterns depending on the strength of bioirrigation σ. The stationary structure changes from homogeneous distributions with low bacteria density via a hot-spot pattern, a striped pattern, and a cold-spot pattern to a homogeneous profile with high bacteria density.

zones of high bacteria density ("hot spots") evolves instead. At higher values of σ we obtain banded structures in the equilibrium. A further increase of the parameter induces the evolution of a pattern, being qualitatively the inverse of the "hot-spots" structure. Thus it can be referred to as "cold-spots" pattern. Finally, if the nutrient can inflow easily, a homogeneous distribution characterized by a high population density of bacteria is stable.

In another series, we study how the model behaves if we do not select a homogeneous steady state as the initial condition but start with a homogeneous distribution, that oscillates. In this case diffusion also can cause the formation of patterns. Generally, the model converges to a stationary inhomogeneous state, as we have presented so far. Nevertheless, we also found parameter sets for the model, leading to the evolution of spatio-temporal patterns. In particular we observed a special kind of oscillation: All points of the domain oscillate with almost the same period, amplitude, and phase, so that the structure of the evolved pattern does not alter, whereas the magnitude of the distribution is pulsating. We tracked this special behavior of the model over a long time. In most cases the dynamics are very stable but transient: The amplitude of oscillations decreases very slow. Thus in the long-term limit a stationary inhomogeneous pattern evolves. In a very small region of parameter space, the oscillations seem to be stable. This region is close to a Turing-Hopf bifurcation. The behavior of reaction-diffusion systems in the neighbourhood of Turing-Hopf bifurcations has been a topic of high interest in recent years [25, 8, 30, 17, 22, 23], and fundamental results have been revealed for the Brusselator. For our sediment model a stable spatio-temporal pattern seems to appear but we leave a detailed Turing-Hopf analysis as a task for future work [2].

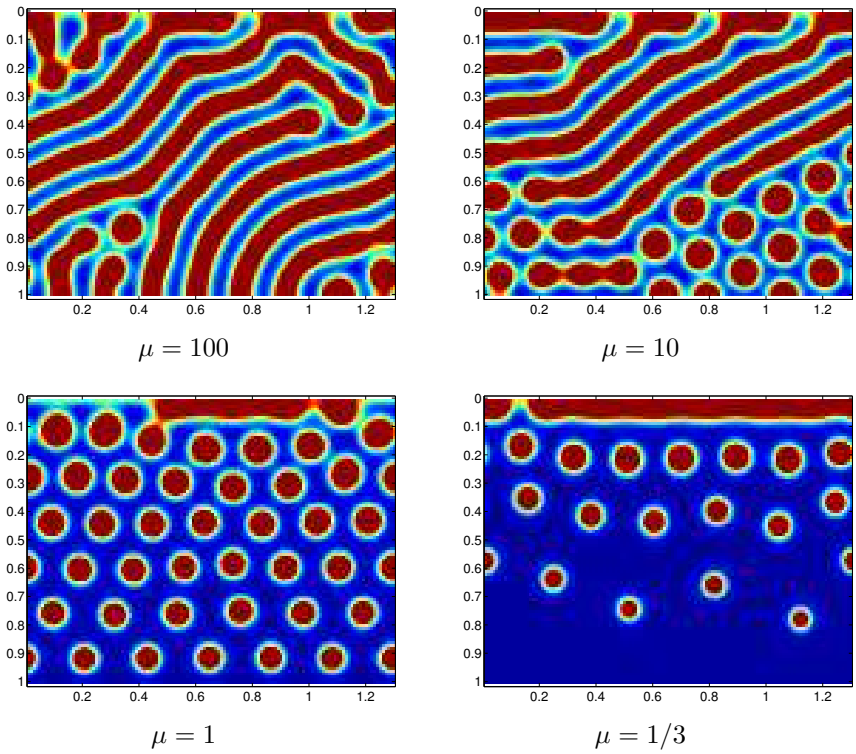

FIGURE 11. Steady states of the sediment model for different bioirrigation functions (population densities of bacteria are plotted). For $\mu = 100$ the bioirrigation acts almost constant on the whole domain. By decreasing μ we retard the inflow of nutrient in the lower parts of the domain. In that region other types of patterns evolve.

4.2.2. *Models forced by nonuniform bioirrigation.* A second series of simulations was performed to study the effect of nonconstant forcing. For that purpose we replace the constant σ by an exponential function decreasing with increasing depth:

$$\sigma(z_v) := \sigma \exp(-z_v/\mu), \tag{26}$$

with μ being a characteristic penetration depth. Since the depthdependency of bioirrigation decreases with parameter μ, we can study the effect of the forcing's nonhomogenity by comparing the long-term profiles of models in which a fixed parameter set (here set 1 with $\gamma = 0.25$) and different values of μ were considered. Fig. 11 shows the results: If μ takes a large value (e.g., $\mu = 100$) the profile does not differ much from those obtained with homogeneous forcing (cf. Fig. 9). Decreasing μ we find that the domain splits up into two zones. The upper one shows stripes, the lower one hot spots. Below certain values of μ (e.g., at $\mu = 1$), the upper zone degenerates to a thin stratum of high bacteria abundance at the top of the domain; below that only hot spots can be found. If we decrease μ further, a third zone establishes at the bottom of the domain, in which the bacteria are almost extinct. This zone exhibits no structures but is homogeneous.

Decreasing the value of δ_x makes it possible to obtain all three types of patterns in one profile. The decrease of σ results in the effect that four of the five stages illustrated in Fig. 10 occur in one steady state (Fig. 12).

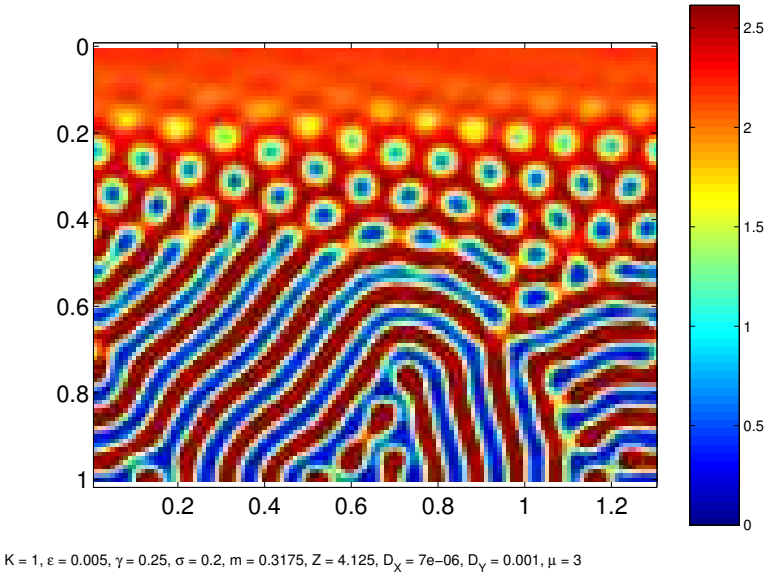

FIGURE 12. Population density of bacteria in a steady state. The profile shows a sequence of four of the five different types of patterns that we presented in Fig. 10.

5. **Discussion.** In a simplified model, we study the dynamics of a population of microorganisms and its nutrient in the sediment. The fundamental processes we consider in the system are degradation of nutrients, affecting the growth of the bacteria's population, inflow and loss of bacteria, inflow of nutrient due to bioirrigation and—as local transport process—diffusion. As experimental studies show, we have to take into account, that the subject bacteria possess an active as well as an inactive state. In the latter, they do not contribute to degradation. In our approach we take into account that the active bacteria can intensify the activation of dormant cells by excreting signal molecules. Another special feature of our model is associated with bioirrigation, which acts as a nonlocal transport of nutrients. Thus our model is globally coupled in space.

First we studied the local dynamics of the two species predator-prey model: Since we presume that nutrients and bacteria flow into the system, it is guaranteed that none of the species becomes extinct. In the local model, at least one nontrivial equilibrium is always found. In general, this steady state is attracting. This means that in almost all cases the system converges to a state in which the concentration of the nutrient and the population density of the bacteria do not alter. However, there are some special cases in which the attractor turns to a repelling focus because of a Hopf bifurcation, and the model shows oscillations in the long-term limit. In large regions of the parameter space, the attracting equilibrium is accompanied by two other steady states, one a saddle and the other an attractor. To illustrate the different behaviours of the models, we choose two different parameter sets and

perfom a variation of the parameter γ. This parameter limits the effect of autocatalytic activation of bacteria and acts as a measure for the nonlinearity of the system.

The main result presented in this paper is the analysis of pattern formation processes due to the interaction of nonlinear growth processes of the bacteria and diffusive transport. We showed that by generalizing the equilibria of the local model we can determine all homogeneous steady-state solutions of a spatial system in a 2D horizontal and vertical domain. If these homogeneous equilibria are stable in the local formulation they may lose this stability with respect to perturbations of certain wavelengths and converge to heterogeneous distributions of bacteria. The conditions to obtain such Turing instabilities inducing pattern formation have been analyzed for this particular model: (i) The particles of the nutrient have to be more mobile than the individual cells of the bacteria; and (ii) the growth of bacteria has to be autocatalytic. Both properties can be considered realistic in sediments: The first follows from the fact that the nutrient particles are much smaller compared to the individual cells of the microorganisms. Additionally, the bacteria tend to stick on the sediment matrix. Condition (ii) is a special feature of the activation mechanism of bacteria, which is taken into account. It is important to note that Turing instability conditions appear in biogeochemical processes in the sediment in a natural way, while in normal chemical processes they are very difficult to achieve.

Performing computer simulations, we found that three types of different non-homogeneous patterns may be stationary in uniformly forced models. In particular, we obtain hot-spot patterns, structures with stripes, or cold-spot patterns. For models with spatially constant bioirrigation, we identified the strength of the influence of bioirrigation (given by parameter σ) as one of the factors that controls what type of pattern is realized. Using this result we performed another series of simulations to study the effect of a non-constant bioirrigation. If we presume that the effect of bioirrigation decreases with increasing depth, we see that different types of patterns, arranged in a vertical sequence, can occur in a stationary state. Such patterns qualitatively resembleexperimentally observed spatial distributions of the activity of bacteria in the sediment [3].

According to our studies inhomogeneous distributions of chemicals and microorganisms in the sediment can develop on domains that are totally uniform with respect to their material properties. The interaction of reaction and diffusion can induce pattern formation. Besides diffusion there are other processes that can influence the emergence of spatial patterns in the sediment, which are not taken into account here. Such processes include advection, chemotaxis and the competition between different degradation pathways. Future works will focus on these additional processes.

Acknowlodgments. We thank W. Ebeling and T. Gross for discussions. This work was supported by the *Deutsche Forschungsgemeinschaft* research group *Bio-GeoChemistry of Tidal Flats.*

References.

[1] M. Baurmann and U. Feudel. Turing patterns in a simple model of a nutrient-microorganism system in the sediment. *Ecological Complexity*, 1(1):77–91, 2004.

[2] M Baurmann, T. Gross, and U. Feudel. Interaction of Hopf- and Turing-bifurcations in 2-species predator-prey systems with diffusional transport. To be published, 2004.

[3] K. Bosselmann, M.E. Böttcher, M. Billerbeck, E. Walpersdorf, A. Theune, D. de Beer, M Hüttel, H.-J. Brumsack, and B.B. Jørgensen. Iron-sulfur-manganese dynamics in intertidal surface sediments in the North Sea. In J. Rullkötter, editor, *BioGeoChemistry of Tidal Flats*, number 12, pages 32–35, Wilhelmshaven, 2003. Forschungszentrum Terramare.

[4] A. Bruns, U Nübel, H. Cypionka, and J. Overmann. Effect of signal compounds and incubation conditions on the culturability of freshwater bacterioplankton. *Applied and Environmental Microbiology*, 69(4):1980–1989, 2003.

[5] U. Bruns, H. Cypionka, and J. Overmann. Cyclic AMP and acryl homoserine lactones increase the cultivation efficiency of heterotrophic bacteria from the central baltic sea. *Applied and Environmental Microbiology*, 68(8):3978–3987, 2002.

[6] S. Camazine, J.-L. Deneubourg, N.R. Franks, J. Sneyd, G. Theraulaz, and E. Bonabeau. *Self-Organization in Biological Systems*. Princeton University Press, Princeton, 2001.

[7] V. Castets, E. Dulos, J. Boissonade, and P. De Kepper. Experimental evidence of a sustained standing Turing-type nonequilibrium chemical pattern. *Physical Review Letters*, 64(24):2953–2956, June 1990.

[8] A. De Wit, D. Lima, G. Dewel, and P. Borckmans. Spatiotemporal dynamics near a codimension-two point. *Physical Review E*, 54(1):261–271, 1996.

[9] B.I. Henry and S.L. Wearne. Existence of Turing instabilities in a two-species fractional reaction-diffusion system. *SIAM journal on applied mathematics*, 62 (3):870–887, 2002.

[10] K.S. Hunter, Y. Wang, and P. VanCappellen. Kinetic modeling of microbially-driven redox chemistry of subsurface enviroments: Coupling transport, microbial metabolism and geochemistry. *Journal of Hydrology*, (209):53–80, 1997.

[11] W. Just, M. Bose, S. Bose, H. Engel, and E. Schöll. Spatiotemporal dynamics near a supercritical Turing-Hopf bifurcation in a two-dimensional reaction-diffusion system. *Physical Review E*, 64(026219):1–12, 2001.

[12] S. Kitsunezaki. Interface dynamics for bacterial colony formation. *Journal of Physical Society of Japan*, 66:1544–1550, 1997.

[13] S.P. Kuznetsov, E. Mosekilde, G. Dewel, and P. Borckmans. Absolute and convective instabilities in a one dimensional Brusselator flow modell. *Journal of Chemical Physics*, 106(18):7609–7616, 1997.

[14] Y.A. Kuznetsov and V.V. Levitin. Content: A multiplatform environment for analyzing dynamical systems. Dynamical Systems Laboratory, Centrum voor Wiskunde en Informatica, Amsterdam, 1996.

[15] S. Madani, F.J.R. Meysman, and J.J. Middelburg. Biogeochemical modeling of sediments from the Santa Barbara Basin (California). In J. Rullkötter, editor, *BioGeoChemistry of Tidal Flats*, number 12, pages 91–93, Wilhelmshaven, 2003. Forschungszentrum Terramare.

[16] H. Malchow. Räumliche und raumzeitliche Strukturbildung in Reaktionssystemen mit Diffusion und Advektion. In J.A. Freund, editor, *Dynamik, Evolution, Strukturen*, pages 229–236. Verlag Dr. Köster, Berlin, 1996.

[17] M. Meixner, A. De Wit, S. Bose, and E. Schöll. Generic spatiotemporal dynamics near codimension-two Turing-Hopf bifurcations. *Physical Review E*, 55

(6):6690–6697, 1997.

[18] Z.J. Mudryk, B. Podgórska, A. Ameryk, and J Bolałek. The occurence and activity of sulphate-reducing bacteria in the bottom sediments of the gulf of Gdańsk. *Oceanologia*, 42(1):105–117, 2000.

[19] J.D. Murray. *Mathematical Biology*. Springer, Berlin, 2 edition, 1993.

[20] G. Nicolis. *Introduction to Nonlinear Science*. Cambridge University Press, Cambridge, 1995.

[21] G. Nicolis and I. Prigogine. *Self-Organization in Nonequilibrium Systems – From Dissipative Structures to Order through Fluctuations*. John Wiley & Sons, New York, 1977.

[22] B. Peña and C. Pérez-García. Stability of Turing patterns in the Brusselator model. *Physical Review E*, 64:056213 1–9, 2001.

[23] B. Peña, C. Pérez-García, A. Sanz-Archelergues, D.G. Míguez, and A.P. Muñuzuri. Transverse instabilities in chemical Turing patterns of stripes. *Physical Review E*, 68:056206 1–7, 2003.

[24] S. Petrovskii, B.-L. Li, and H. Malchow. Quantification of the spatial aspect of chaotic dynamics in biological and chemical systems. *Bulletin of Mathematical Biology*, 65(3):425–446, 2003.

[25] A. Rovinsky and M. Menzinger. Interaction of Turing and Hopf bifurcations in chemical systems. *Physical Review A*, 46(10):6315–6322, 1992.

[26] A.B. Rovinsky and M. Menzinger. Differential flow instability in dynamical systems without an unstable (activator) subsystem. *Physical Review Letters*, 72(13):2017–2020, 1994.

[27] R.A. Satnoianu, P.K. Maini, and M. Menzinger. Parameter space analysis, pattern sensitivity and model comparison for Turing and stationary flow-distributed waves (FDS). *Physica D*, (160):79–102, 2001.

[28] R.A. Satnoianu, M. Menzinger, and P.K. Maini. Turing instabilities in general systems. *Mathematical Biology*, 41(6):493–512, 2000.

[29] R.A. Satnoianu, J.H. Merkin, and S.K. Scott. Spatio-temporal structures in a differential flow reactor with cubic auto catalator kinetics. *Physica D*, (124): 345–367, 1998.

[30] M. Tlidi, P. Mandel, and M. Haelterman. Spatiotemporal patterns and localized structures in nonlinear optics. *Physical Review E*, 56(6):6524–6530, 1997.

[31] L. Tsimring, H. Levine, I. Aranson, E. Ben-Jacob, I. Cohen, O. Shochet, and W.N. Reynolds. Aggregation patterns in stressed bacteria. *Physical Review Letters*, 75(9):1859–1862, 1995.

[32] A.M. Turing. The chemical basis of morphogenisis. *Philosophical transactions of the Royal Society of London - B*, 237(B 641):37–72, 1952.

[33] P. VanCappellen and Y. Wang. Cycling of iron and maganese in surface sediments: A general theory for the coupled transport and reaction of carbon oxygen, nitrogen, sulfur, iron and maganese. *American Journal of Science*, 296:197–243, 1996.

Received on March 2, 2004. Revised on March 22, 2004.

E-mail address: baurmann@icbm.de
URL: http://www.icbm.de/komplsyst/index.html